View Online

The importance of ion size and electrode curvature on electrical double layers in ionic liquids

Guang Feng,[a] Rui Qiao,*[a] Jingsong Huang,[b] Sheng Dai,[b] Bobby G. Sumpter[b] and Vincent Meunier[c]

Received 7th October 2010, Accepted 21st October 2010
DOI: 10.1039/c0cp02077j

Downloaded by University of Tennessee at Knoxville on 26 November 2010
Published on 15 November 2010 on http://pubs.rsc.org | doi:10.1039/C0CP02077J

Room-temperature ionic liquids (ILs) are an emerging class of electrolytes for supercapacitors. We investigate the effects of ion size and electrode curvature on the electrical double layers (EDLs) in two ILs 1-butyl-3-methylimidazolium chloride [BMIM][Cl] and 1-butyl-3-methylimidazolium hexafluorophosphate [BMIM][PF_6], using a combination of molecular dynamics (MD) and quantum density functional theory (DFT) simulations. The sizes of the counter-ion and co-ion affect the ion distribution and orientational structure of EDLs. The EDL capacitances near both planar and cylindrical electrodes were found to follow the order: [BMIM][Cl] (near the positive electrode) > [BMIM][PF_6] (near the positive electrode) ≈ [BMIM][Cl] (near the negative electrode) ≈ [BMIM][PF_6] (near the negative electrode). The EDL capacitance was also found to increase as the electrode curvature increases. These capacitance data can be fit to the Helmholtz model and the recently proposed exohedral electrical double-cylinder capacitor (xEDCC) model when the EDL thickness is properly parameterized, even though key features of the EDLs in ILs are not accounted for in these models. To remedy the shortcomings of existing models, we propose a "Multiple Ion Layers with Overscreening" (MILO) model for the EDLs in ILs that takes into account two critical features of such EDLs, *i.e.*, alternating layering of counter-ions and co-ions and charge overscreening. The capacitance computed from the MILO model agrees well with the MD prediction. Although some input parameters of the MILO model must be obtained from MD simulations, the MILO model may provide a new framework for understanding many important aspects of EDLs in ILs (*e.g.*, the variation of EDL capacitance with the electrode potential) that are difficult to interpret using classical EDL models and experiments.

1. Introduction

Room-temperature ionic liquids (ILs) have attracted significant attention in fundamental and applied research in recent years. The extensive interest is in part due to their wide electrochemical windows, excellent thermal stability, non-volatility, relatively inert nature, and good ionic conductivity, which make ILs exceptionally useful in diverse electrochemical devices.[1] In particular, ILs are a promising candidate as electrolytes in electrical double layer capacitors (EDLCs, also called supercapacitors). EDLCs constitute an attractive class of energy storage devices owing to their high power density, excellent durability, and good performance at relatively low temperature.[2,3] Since EDLCs store energy physically in the electrical double layer (EDL) near the electrodes, it is necessary to develop a detailed understanding of EDLs at the interface between ILs and electrodes to optimize their use in EDLCs.

ILs are composed exclusively of organic cations and organic/inorganic anions.[4,5] The nature of cations/anions plays a key role in determining the physicochemical properties of ILs, and consequentially affects the structure and capacitance of EDLs in ILs. The structure and capacitance of EDLs in ILs have been studied by several research groups recently.[6] For example, Pinilla and co-workers investigated the molecular arrangement of [DMIM][Cl] near electrified walls.[7] Fedorov and Kornyshev studied the EDLs in ILs modeled by charged Lennard-Jones spheres and found that the cation/anion size asymmetry affects the trend of differential capacitance.[8] Using molecular dynamics (MD) simulations, we examined the EDLs in [BMIM][NO_3] near planar electrodes and found that the correlation between anion and cation played a key role in determining the ion distribution and the EDL capacitance.[9] Sedev and colleagues found experimentally that the differential capacitance increased in the order [HMIM][Cl] < [BMIM][Cl] < [EMIM][Cl] due to the different cation sizes.[10] These studies improved the understanding of how the nature of ILs affects the EDL. However, a systematic molecular level study of how ion size affects the EDL structure and capacitance is still lacking at present. In addition, up to now, a detailed atomistic study of the influence of electrode curvatures on the EDLs in ILs has not been reported yet.

A fundamental understanding of the effects of ion size and electrode curvature on EDLs in ILs can benefit from a realistic

[a] *Department of Mechanical Engineering, Clemson University, Clemson, South Carolina, 29634-0921, USA. E-mail: rqiao@clemson.edu; Web: http://clemson.edu/~rqiao*
[b] *Oak Ridge National Laboratory, Bethel Valley Road, Oak Ridge, Tennessee 37831-6367, USA*
[c] *Department of Physics, Applied Physics, and Astronomy, Rensselaer Polytechnic Institute, Troy, New York 12180-3590, USA*

View Online

Downloaded by University of Tennessee at Knoxville on 26 November 2010
Published on 15 November 2010 on http://pubs.rsc.org | doi:10.1039/C0CP02077J

model of EDLs, and *vice versa*. Currently, the most widely used model is the Helmholtz model, in which the IL-electrode interface is hypothesized to be one ion-layer thick.[11] Although this model seems to be supported by some experimental characterizations of EDLs, most MD simulations suggest that alternating layers of counter-ions and co-ions penetrate deep (>1 nm) into the electrolyte.[9,12,13] More advanced models, *e.g.* the ones proposed by Kornyshev[14] and Oldham,[15] assumed that the EDLs in ILs are made of a Helmholtz-like inner layer and a "diffusive" outer layer. Although these elegant models capture the structure of EDLs better, and can predict qualitatively the experimentally observed capacitance–potential correlations, they are mostly mean-field theories and cannot depict some key aspects of EDL in ILs, *e.g.* alternating layering of counter-ions and co-ions and the overscreening of electrode charge in the EDL.[16,17]

The goal of this work is to establish how the ion size and electrode curvature influence the microstructure and capacitance of the EDLs at IL/electrode interfaces. To this end, we used both classical MD and first-principles methods to model ILs and planar/cylindrical electrodes with chemical details. The results indicate that anion size and electrode curvature play an important role in the cation distribution in EDLs and that charge overscreening is a universal feature of EDLs in ILs. Following these results, we further develop a new model for EDLs in ILs and test the model using our MD data. The rest of this paper is organized as follows: the simulation system and methods are presented in Section 2; the microstructure of EDLs are discussed in Sections 3; the results on the EDL capacitance are given, and the existing classical models for EDLs are examined in Section 4; a new model for EDLs in ELs is proposed and tested in Section 5. Finally, the conclusions are presented in Section 6.

2. Simulation system and methods

We performed MD simulations of ILs in contact with planar and cylindrical exohedral[18] electrodes modeled by graphene sheets and carbon nanotubes (CNTs). In the planar electrode simulations, ILs are enclosed between two planar electrodes and each wall was modeled as a graphene sheet (see Fig. 1a). The gap between two electrodes was set to 6.0 nm to produce a bulk-like behavior in the channel center. The size of the simulation box was 5.94 nm in both x- and y-directions. The coordinate system is defined such that $z = 0$ corresponds to the geometrical plane of the lower electrode. In the cylindrical electrode simulations, a (5,5) CNT with a diameter of 0.67 nm was placed at the center of a box of ILs (see Fig. 1b). The length of CNT is 6.1 nm, pointing along z, and the size of simulation box along x- and y-directions was set to 6.0 nm, which is large enough to obtain a bulk-like behavior at position far from the CNT. Three different surface charge densities (0, +0.112, and −0.112 C m^{-2}) were studied by assigning a net partial charge to the atoms of the electrode. [BMIM][Cl] and [BMIM][PF_6] were chosen as ILs due to their different anion size (the diameter of the Cl^- and PF_6^- ions are 3.62 Å and 5.10 Å, respectively[19]). The force fields for the electrode atoms (carbon) were taken from ref. 20. The force fields for the $BMIM^+$ and PF_6^- ions were taken from ref. 21, and the force field for the Cl^- ions was taken from ref. 22. Periodic boundary conditions were applied in x- and y-directions for simulations with planar electrodes, and in all three dimensions for simulations with CNT electrodes.

Simulations were performed in the NVT ensemble using an MD package Gromacs.[23] For each simulation, the number of ions in the system was tuned such that the ion concentration of the bulk-like region in the simulation box matched that of the bulk ILs. The PME method was used to compute the electrostatic interactions. Specifically, an FFT grid spacing of 0.12 nm and cubic interpolation for charge distribution were used to compute the electrostatic interactions in reciprocal space. A cutoff distance of 1.0 nm was used in the calculation of electrostatic interactions in the real space. The nonelectrostatic interactions were computed by direct summation with a cutoff length of 1.0 nm. The LINCS algorithm[24] was used to maintain the bond length of the $BMIM^+$ and PF_6^- ions. In each simulation, we first heated the system to 1000 K, and then annealed to 365.15 K in 3 ns. The system was then allowed to equilibrate for another 6 ns to obtain an equilibrium state. Finally, a 50 ns production run was performed. To ensure

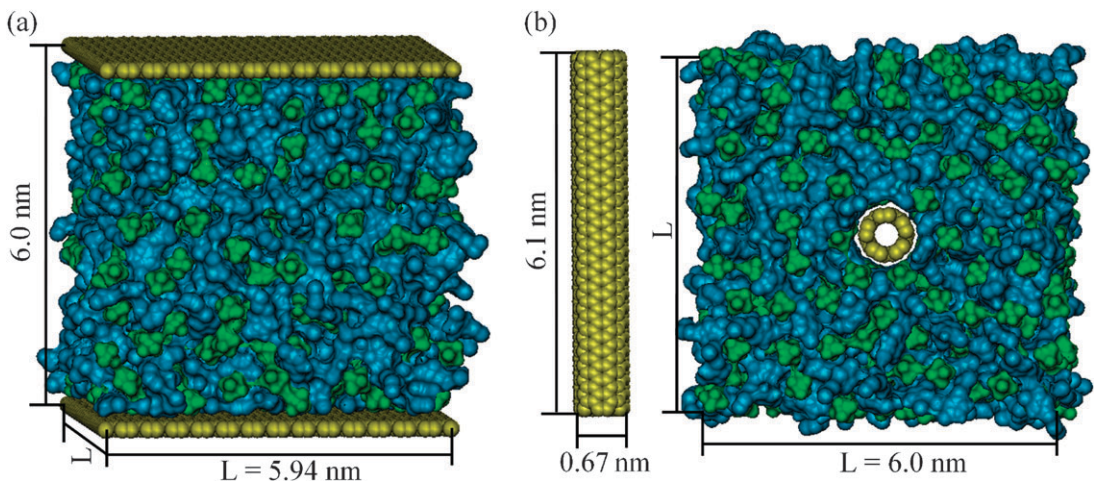

Fig. 1 Snapshots of simulation systems with graphene sheets (panel a) and CNT (panel b) as electrodes. The blue, green, and yellow spheres represent $BMIM^+$ ions, PF_6^- ions, and electrode atoms.

 This journal is © the Owner Societies 2010

View Online

Downloaded by University of Tennessee at Knoxville on 26 November 2010
Published on 15 November 2010 on http://pubs.rsc.org | doi:10.1039/C0CP02077J

statistical accuracy, each simulation case was repeated five times with different initial configurations.

The microstructure of the EDL, *e.g.* ion number density and space charge density profiles, was computed using the binning method. The capacitance of the EDL was computed by[25]

$$C_{\mathrm{EDL}} = \frac{\sigma}{\phi_{\mathrm{EDL}} - \mathrm{PZC}}, \qquad (1)$$

where ϕ_{EDL} is the potential drop across the EDL, and PZC is the potential difference between a neutral electrode and the bulk electrolyte. In the planar electrode simulations, the potential distribution was obtained using the method in ref. 26. In the cylindrical electrode simulations, the potential distribution was calculated by

$$\phi(r) = -\frac{1}{\varepsilon_0}\left[\int_R^r u\rho_e(u)\ln\frac{r}{u}\mathrm{d}u + R\sigma\ln\frac{r}{R}\right], \qquad (2)$$

where R and ε_0 are the radius of cylindrical electrode and vacuum permittivity, respectively. $\rho_e(u)$ is the space charge density in the radial direction. In this work, the PZCs of the planar and CNT electrodes in contact with [BMIM][Cl] were found to be 414 mV and 458 mV, respectively. The former PZC value is very close to the 420 mV reported in a recent experimental study.[10] The PZCs of the planar and CNT electrodes in contact with [BMIM][PF_6] are both essentially zero. The PZC at planar electrode is consistent with that reported for graphite surface in a recent MD simulation study.[27]

In order to obtain fundamental information that includes important quantum effects related to the confined geometries at EDLs, we carried out large-scale quantum density functional theory (DFT) calculations. All DFT calculations were performed using the periodic DFT program Vienna *ab initio* simulation package (VASP), version 4.6.[28–31] The Kohn-Sham equations were solved using the projector augmented wave (PAW) approach[32,33] within the frozen core approximation to describe the electron–core interaction and a plane wave basis set. The basis was composed of plane-waves up to a 400 eV kinetic energy cutoff. In each case the total electronic self-consistent field (SCF) was converged to 10^{-4} eV per molecule. Unless otherwise stated, the generalized gradient approximation (GGA) exchange-correlation functional of Perdew, Burke, and Ernzerhof (PBE)[34] was utilized. Electronic convergence was defined as a consistency between successive cycles of less than 10^{-5} eV. Each CNT system (neutral CNT + exohedral IL) was placed in a cell that ensured at least 12 Å of vacuum in the two non-periodic directions between the CNT and its reflection. For single IL exohedral adsorption, the IL ($BMIM^+$ cation alone or the $BMIM^+$ and PF_6^- cation–anion pair) was positioned on the CNT such that the periodic images along the CNT axis were 12 Å apart. The 1D Brillouin zone was sampled using a string of 16 k-points, a sampling that was found to be sufficient to attain good numerical convergence. The binding energy for IL adsorption was computed by the difference between the total system and the infinitely separated ILs and CNT. To explore adsorption of the ILs inside a graphene slit, a model as depicted in Fig. 1a was used (2 graphene sheets separated by a fixed distance at 1.2 nm for the DFT calculations). In this case we only considered the adsorption of a single $BMIM^+$ cation at one of the neutral surfaces.

3. Ion distribution in EDLs

For the distribution of $BMIM^+$, Cl^-, and PF_6^- ions and the orientation of $BMIM^+$ ions near neutral and electrified electrodes, we found general trends similar to those reported earlier, regardless of the electrode curvature. For example, (1) $BMIM^+$ ions adsorb significantly on neutral and negatively charged electrodes.[9,27,35–37] The first peak of their concentration profile is systematically located ~0.347 nm from the electrode surface. Such a distance remains virtually the same if the system consists of only a single $BMIM^+$ ion and the electrodes. From the DFT calculations, a $BMIM^+$-surface distance of 3.44 Å was determined for a (9,0) CNT and 3.40 Å inside a defect-free graphene slit, in excellent agreement with MD results. This agreement provides evidence that the model and potentials used in the classical MD simulations adequately capture the essential interactions at the interface. The DFT-computed value for the interaction energy for the $BMIM^+$ cation on the neutral CNT is 0.32 eV, which explains the significant adsorption of $BMIM^+$ on neutral electrodes. Nevertheless, the overall electronic band structure of the CNT is not substantially modified by the adsorption of the $BMIM^+$, in agreement with the absence of Faradic process at the interface of EDLs. (2) The imidazolium ring of $BMIM^+$ ion becomes more parallel to the electrode, as the electrode charge density (σ) becomes more negative, and tends to be more vertical to the electrode, as σ becomes more positive.[7,35] (3) Near neutral electrodes, it was also observed that the neutral tails of $BMIM^+$ ions lie flat on the electrode similar to the imidazolium ring. This is consistent with results reported in earlier MD simulations.[27,38] (4) For charged electrodes, MD simulations indicate that the cations and anions form alternating layers due to the strong cation–anion correlations, and the layering penetrates about 1–1.5 nm into the IL bulk.[9,39] (5) The strong cation–anion correlations also manifest from the co-adsorption of cations and anions on the surface of neutral electrodes. We note that from the DFT calculations, co-adsorption of a cation and an anion onto a neutral CNT leads to a packing where the PF_6^- anion associates to the C2 position of the $BMIM^+$ cation due to the enhanced H-bonding interactions, which is quite common for imidazolium-based ILs.[40–43] (Recent MD simulations on [BMIM][PF_6] found that the hydrogen bonds have short lifetimes as a result of the fast rotations of PF_6^- ions.[44] This effect may have come from thermal effects since the MD simulations were performed at temperatures of 300–380 K compared to 0 K in our DFT calculations.) With an increased amount of cation–anion pairs, the cation–anion correlation leads to a "staggered-pair" packing at the nanotube surface that repeats both around the circumference and along the nanotube axis to give complete coverage. This level of surface coverage tends to completely screen the π–π interactions that cause nanotube agglomeration (formation of bundles) which is the fundamental mechanism underlying the excellent solvent properties of IL for nanotubes and the formation of a bucky-gel.

View Online

Downloaded by University of Tennessee at Knoxville on 26 November 2010
Published on 15 November 2010 on http://pubs.rsc.org | doi:10.1039/C0CP02077J

Below we examine how the anion size affects the EDL structure. As mentioned above, the MD results show excellent agreement with the quantum DFT calculations for the neutral surface cases. This serves as the validation of the potentials, indicating that much larger system size, time scale and parameter space (such as ion size and interface curvature effects) can be examined using the MD approach described in the current paper with good confidence. In the following sections, we report exclusively on results obtained from such calculations.

3.1 Ion size effects

In Fig. 2 we compare the density distribution (ρ_n) of ions in [BMIM][Cl] and [BMIM][PF_6] near neutral planar electrodes. We observe the following trends: (1) Comparing the Cl^- and PF_6^- ion density profiles adjacent to the first peak of the $BMIM^+$ ion profile, Cl^- ions spread in a wider region, but with a lower peak, and the Cl^- ion density peak is closer to the electrode than that of the PF_6^- ions. (2) The second peak of $BMIM^+$ ion profile is closer to the electrode, when the anion is Cl^-. These observations are closely related to the smaller size of Cl^- ions compared to PF_6^- ions. To understand observation 1, we note that the Cl^- ions adsorbed on the electrode (signified by the first peak of Cl^- ion profile) can approach the electrode closer than the PF_6^- ions due to their smaller size. However, the adsorption of PF_6^- ions is much stronger mainly for two reasons. First, the van der Waals force between the electrode atoms and ions, a key driving force for ion adsorption, is stronger for the polyatomic PF_6^- ion than for the monoatomic Cl^- ion. Second, as anions are adsorbed on electrodes, part of the coordination shell (consisting primarily of cations) must be removed due to the spatial confinement imposed by the electrode. Such a partial "desolvation" process tends to hinder their adsorption on the electrode. Since PF_6^- ions are larger than Cl^- ions, a smaller fraction of their coordination shell is removed compared to Cl^- ions as they become adsorbed on the electrodes. Consequently, PF_6^- ions adsorb more strongly on neutral electrodes. The densely packed PF_6^- ions adsorbed on the electrode prevent more PF_6^- ions from approaching them. It follows that we observe a near depletion of PF_6^- ions in region 0.54 to 0.68 nm from the electrode, and such a phenomenon doesn't occur for the loosely packed Cl^- ions adsorbed on the electrode. Observation 2 is caused by the different size of the anions, *i.e.*, the densely packed PF_6^- ions in the first layer adjacent to the electrode prevent the second $BMIM^+$ layer from approaching too closely to the electrode.

In the present study, the polarization of electrodes by ions near them is not modeled and the interactions between ions and these polarization charges (often termed image charge interactions) are not accounted for. The image charge interactions tend to enhance the adsorption of ions, and the enhancement is stronger for the smaller Cl^- ions than for the larger PF_6^- ions. However, we note that the image charge interactions are strongly screened by the ion pairs in the system, and thus the ion adsorption on electrodes is unlikely to be changed significantly by such interactions. This is indirectly supported by classical MD simulations of high-temperature molten salts.[45] In those simulations, the ion distribution near electrodes is only slightly modified when the image charge interactions are included. To what extent the adsorption of room-temperature ILs on electrode is affected by image charge interactions will require a more systematic study.

Fig. 3a and b show the density distribution of ions near planar electrodes with $\sigma = +0.112\ C\ m^{-2}$. A distinct $BMIM^+$ ion layer, located at $z = 0.35$ nm, follows closely the first Cl^- layer (see Fig. 3a). However, such a $BMIM^+$ ion layer is not observed near the first PF_6^- layer in [BMIM][PF_6] (see Fig. 3b). The smaller size of Cl^- ions is responsible for this difference. Specifically, although the adsorption of $BMIM^+$ ions is reduced by the electrostatic repulsion from the electrode, it is facilitated by the strong attraction between the anions and $BMIM^+$ ions. Such an attraction is stronger for the smaller Cl^- ions. In addition, because of their smaller size, Cl^- ions leave more space near the positive electrodes for the $BMIM^+$ ions.

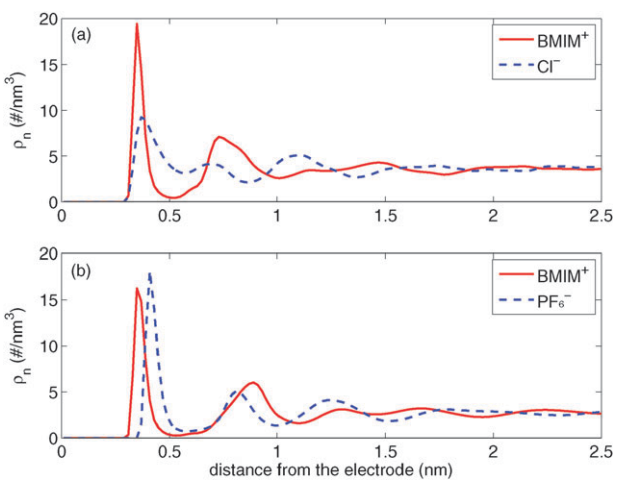

Fig. 2 Ion number density profiles in [BMIM][Cl] (panel a) and [BMIM][PF_6] (panel b) near neutral planar electrodes. The positions of the cation and the anion are represented by the geometrical center of the imidazolium ring and the entire anion, respectively.

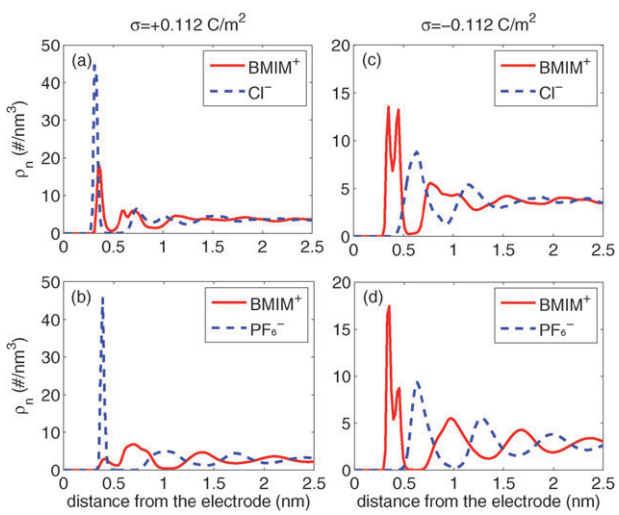

Fig. 3 Ion number density profiles in [BMIM][Cl] (panels a and c) and [BMIM][PF_6] (panels b and d) near positive and negative planar electrodes.

 This journal is © the Owner Societies 2010

View Online

Downloaded by University of Tennessee at Knoxville on 26 November 2010
Published on 15 November 2010 on http://pubs.rsc.org | doi:10.1039/C0CP02077J

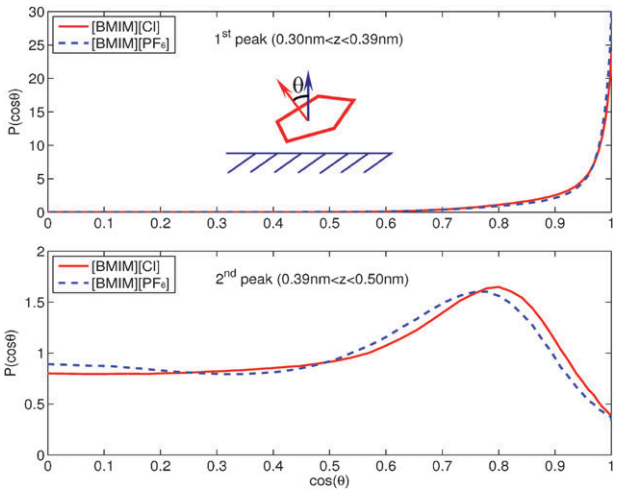

Fig. 4 Distribution of the angle θ formed between the normal of imidazolium ring in the twin-peaks of $BMIM^+$ ion (see Fig. 3c and d) and the normal direction of the electrode with $\sigma = -0.112$ C m^{-2}.

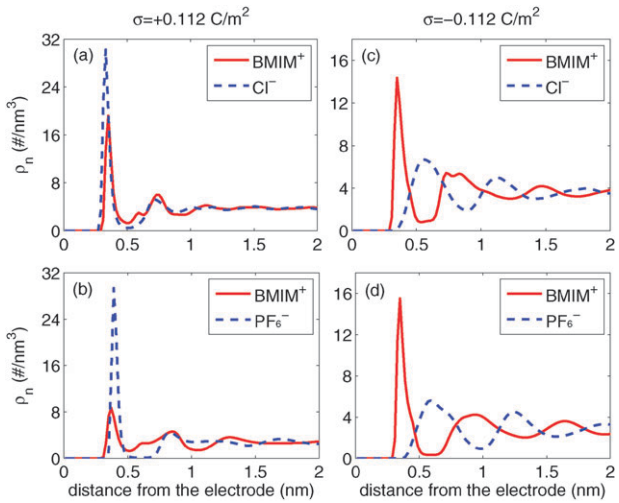

Fig. 5 Ion number density profiles in [BMIM][Cl] (panels a, c) and [BMIM][PF_6] (panels b, d) near positive (panels a, b) and negative (panels c, d) CNT electrodes.

Fig. 3c and d show the number density distribution of ions near planar electrodes with $\sigma = -0.112$ C m^{-2}. We observe that (1) the density profile of $BMIM^+$ ions shows two peaks (a doublet) at $z = 0.35$ nm and $z = 0.45$ nm from the planar electrodes in both Fig. 3c and d, and (2) when Cl^- ion is the anion, the two peaks have similar height. However, when PF_6^- ion is the anion, the second peak becomes much lower than the first peak. To understand observation 1, we analyzed the molecular structure for the systems of Fig. 3c and d and found that the $BMIM^+$ ions in both peaks are contact-adsorbed on the electrode. As shown in Fig. 4, the imidazolium rings of $BMIM^+$ ions in the first peak are almost parallel to the electrode, while those of $BMIM^+$ ions in the second peak become more random. The formation of the doublet, or equivalently the different orientation of contact-adsorbed $BMIM^+$ ions, mainly arises from the incommensurate shape of the "flat" $BMIM^+$ ions and spherical Cl^-/PF_6^- ions. Specifically, the nearly spherical anions accumulated near the first $BMIM^+$ peak can't be packed effectively with the $BMIM^+$ ions adsorbed on the electrode if all $BMIM^+$ ions lie parallel to the electrode. The second observation follows from the fact that more Cl^- ions accumulate in the region (0.44 nm $< z <$ 0.89 nm) very close to the negatively charged electrode, which forces more contact-adsorbed $BMIM^+$ ions to orient less parallel to the electrode to achieve a better packing with the Cl^- ions. The larger accumulation of Cl^- ions in this region is caused by its stronger attraction to the $BMIM^+$ ions than the larger PF_6^- ions.

The above results indicate that the size of anions affects the distribution of cations near both negatively and positively charged electrodes. At the fundamental level, these effects originate from the different attractions between cations and anions with different sizes, which play a key role in determining the ion distribution in EDLs inside ILs.

3.2 Curvature effects

Fig. 5a–d show the ionic density profiles in [BMIM][Cl] and [BMIM][PF_6] near CNT electrodes with $\sigma = \pm 0.112$ C m^{-2}, *i.e.*, the same as for the planar electrodes used in Fig. 3a–d. At $\sigma = +0.112$ C m^{-2}, the peaks of the anion concentration profiles (Cl^- ion in Fig. 5a and PF_6^- ion in Fig. 5b) are much lower than those shown in Fig. 3a and b. In addition, the cation layer near the first peak of anion layer becomes higher (this is especially obvious in Fig. 5b). Near the negative CNT electrodes, the doublet-peaks of $BMIM^+$ ions are replaced by a single peak, and the height of the first anion peak (Cl^- ion in Fig. 5c and PF_6^- ion in Fig. 5d) is not substantially changed. The reduced first counter-ion peak and enhanced first co-ion peak are both caused by the reduced electrical field near exohedral cylindrical electrodes, compared with those near planar electrode with the same σ. Specifically, Gauss' law predicts that at the same distance from the electrode with the same σ, the electric field is weaker near cylindrical electrodes than near planar electrodes. This leads to a reduced driving force for the counter-ion adsorption and co-ion desorption on the electrode, which in turn leads to the above observations.

4. Ion size and curvature effects on EDL capacitance

4.1 Results

Fig. 6 shows the capacitance of EDLs with surface charge densities of $\sigma = \pm 0.112$ C m^{-2} for different counter-ion/co-ion and electrode geometries. We note that the capacitance of EDLs in [BMIM][PF_6] is similar to that reported in ref. 35. We observe that near both planar and cylindrical electrodes, the EDL capacitance as a function of the counter-ion type follows the order $Cl^- > PF_6^- \approx BMIM^+$ (PF_6^- as co-ion) $\approx BMIM^+$ (Cl^- as co-ion). Such an order is consistent with the expectation based on the classical Helmholtz model, *i.e.*, EDL capacitance decreases as the counter-ion size increases. Fig. 6 also shows that for EDLs with the same counter-ion and co-ion, the capacitance increases by 30–44% as the electrode shape changes from planar to cylindrical. This enhancement of capacitance due to the electrode curvature is consistent with

View Online

Downloaded by University of Tennessee at Knoxville on 26 November 2010
Published on 15 November 2010 on http://pubs.rsc.org | doi:10.1039/C0CP02077J

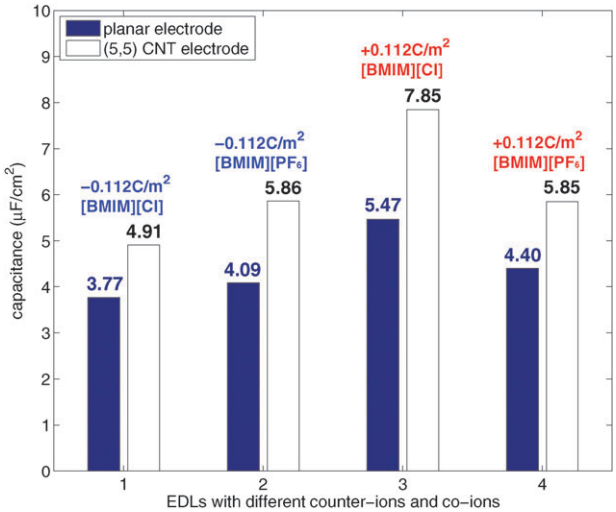

Fig. 6 The capacitance of EDLs near planar and CNT electrodes with $\sigma = \pm 0.112$ C m^{-2} in contact with different ILs. The potential drop across each EDL, from left to right in the figure, is 2.97 V, 2.28 V, 2.74 V, 1.91 V, 2.05 V, 1.43 V, 2.55 V and 1.92 V, respectively.

the prediction by the exohedral electrical double-cylinder capacitor (xEDCC) model,[46] *i.e.*, for the same EDL thickness, the capacitance increases with increased electrode curvature. The above results demonstrate that the dependence of EDL capacitance on the ion size and electrode geometry is in qualitative agreement with available theories. However, to use these models to guide the optimization of EDL capacitance by exploiting ion specificity and electrode curvature effects, the accuracy of these models must be examined quantitatively. Below, we use the data from Fig. 6 to examine the Helmholtz and xEDCC models.

4.2 Quantitative examination of Helmholtz and xEDCC models

Based on the Helmholtz model, the capacitance of an EDL near a planar electrode, C_∞, is given by

$$C_\infty = \frac{\varepsilon_\infty}{d_\infty}, \tag{3}$$

where ε_∞ and d_∞ are the permittivity and thickness of the Helmholtz layer. Based on the xEDCC model, the capacitance of an EDL near an exohedral cylindrical electrode, C_c, is given by[46]

$$C_c = \frac{\varepsilon_c}{R\ln\left(1+\frac{d_c}{R}\right)}. \tag{4}$$

Here, ε_c is the permittivity in the EDL, d_c is the separation between the counter-ion layer and the electrode surface, and R is the radius of the exohedral cylindrical electrode. In principle, the accuracy of eqn (3) and (4) can be studied by comparing their prediction of C_∞ and C_c with simulation data. In practice, such a comparison is not straightforward. Specifically, although d_∞ and d_c can be measured in MD simulations or experiments, ε_∞ and ε_c are difficult to obtain. In fact, the permittivity at the interface of fluid/electrode in the direction normal to the electrode is extremely difficult to compute.[47] At present, only the static dielectric constant in bulk ILs can be measured with accuracy,[48,49] and experimental measurement of the dielectric constant of interfacial ILs has not been reported yet. Hence, it's unclear whether the dielectric constant in the EDL is the same as that in the bulk ILs. However, it is well-known that, for the EDLs in aqueous electrolytes, the dielectric constant in the Helmholtz layer can be 5 to 10 times smaller than in bulk electrolytes.[50–53] The direct evaluation of eqn (3) and (4) is difficult since it requires a precise permittivity value in the EDL. To avoid this difficulty, we test these models by examining the enhancement of EDL capacitance (η) due to increased electrode curvature, *i.e.*, we compute η as

$$\eta = C_c/C_\infty = \frac{\varepsilon_c}{\varepsilon_\infty}\frac{d_\infty}{R\ln(1+d_c/R)}. \tag{5}$$

Here we assume that $\varepsilon_c \approx \varepsilon_\infty$, *i.e.*, the dielectric permittivity is the same for ILs near electrodes with different curvatures at the same surface charge density. Although this assumption is not ideal, it's far less restrictive than other assumptions such as assuming $\varepsilon_c \approx \varepsilon_{bulk}$. With this proviso, we obtain

$$\eta = C_c/C_\infty = d_\infty/R\ \ln(1 + d_c/R). \tag{6}$$

Testing the accuracy of eqn (6) requires the thickness of the EDL, *i.e.*, d_∞ and d_c, as input parameters. However, d_∞ and d_c can be identified without ambiguity only when three conditions are met simultaneously, *i.e.*, (a) the electrode charge is screened exactly by a single layer of counter-ions, (b) the electric charge of each counter-ion is centered on a single atom, and (c) there is no charge separation in the electrolyte near neutral electrodes. However, the ion concentration profiles (see Fig. 2, 3 and 5) and the delocalized nature of the ion's charge in ILs indicate that none of these conditions is rigorously satisfied for the EDLs in ILs. Consequently, there are several possible choices when evaluating EDL thickness from MD data. Specifically, if the number density profiles of counter-ions and net charge density profiles near electrodes with a surface charge density of σ, *i.e.*, $\rho^\sigma_{n,\text{counter-ion}}$ and ρ^σ_e, are given, then the EDL thickness near a charged electrode may be obtained from:

1. the distance between the first peak of $\rho^\sigma_{n,\text{counter-ion}}$ and the electrode surface, *i.e.*, the EDL thickness is based on ρ^σ_n;
2. the distance between the first peak of the profile $\Delta\rho^\sigma_{n,\text{counter-ion}} = \rho^\sigma_{n,\text{counter-ion}} - \rho^0_{n,\text{counter-ion}}$ to the electrode surface, *i.e.*, the EDL thickness is based on $\Delta\rho^\sigma_n$; or
3. the distance between the first peak of the profile $\Delta\rho^\sigma_e = \rho^\sigma_e - \rho^0_e$ to the electrode surface, *i.e.*, the EDL thickness is based on $\Delta\rho^\sigma_e$.

The first option is the most frequently adopted choice in the literature. It amounts to neglecting the ion charge delocalization, the ion adsorption on neutral electrodes, and the charge separation beyond the first counter-ion layer. With the second option, the ion charge delocalization and the charge separation beyond the first counter-ion layer are ignored. The third option is equivalent to neglecting the charge separation beyond the first space charge density peak. The capacitance predicted by eqn (6) using EDL thickness following choices 1 and 2 are similar. For brevity, we present the examination of eqn (6) using EDL thickness defined with choices 2 and 3. Fig. 7a–d show $\Delta\rho^\sigma_n$ and $\Delta\rho^\sigma_e$ for [BMIM][Cl] adjacent to

 This journal is © the Owner Societies 2010

View Online

Downloaded by University of Tennessee at Knoxville on 26 November 2010
Published on 15 November 2010 on http://pubs.rsc.org | doi:10.1039/C0CP02077J

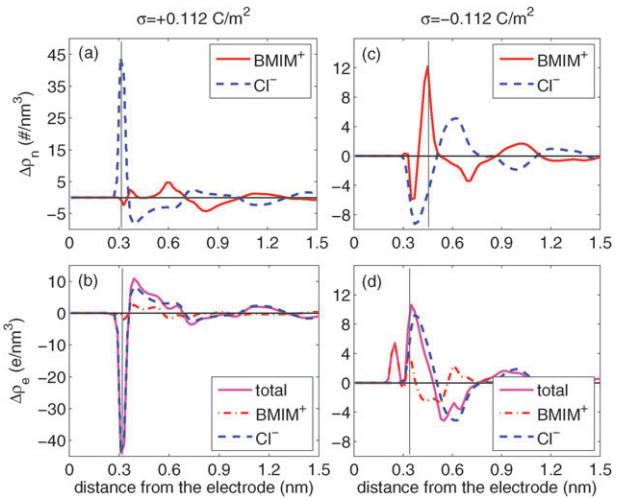

Fig. 7 Change of ion number densities (panels a and c) and space charge densities (panels b and d) in [BMIM][Cl] near planar electrodes as the electrode charge density is changed from zero to ± 0.112 C m^{-2}.

planar electrodes with $\sigma = \pm 0.112$ C m^{-2}. In these figures, $z = 0$ corresponds to the electrode surface. We retrieve d_∞ using the $\Delta\rho_n$ and $\Delta\rho_e$ profiles shown in Fig. 7, and the results are listed in Table 1. Note that when the $\Delta\rho_e$ has two closely-spaced peaks (*e.g.*, in Fig. 7d), the position of an "effective" first peak of the $\Delta\rho_e$ profile is taken as geometrical center of such peaks. Using similar method, d_c for the EDLs in [BMIM][Cl] adjacent to CNT electrodes and $d_\infty(d_c)$ in [BMIM][PF$_6$] adjacent to planar (CNT) electrodes were retrieved and listed in Table 1. With d_∞ and d_c shown in Table 1, η is computed using eqn (6) and the results are summarized in Table 1.

We observe that the relative error in η predicted by eqn (6) using $\Delta\rho_n^\sigma$-based d_∞ and d_c is about 6–31%, while the error in η predicted by eqn (6) using $\Delta\rho_e^\sigma$-based d_∞ and d_c is about 1–10%. These results suggest that EDL thickness based on $\Delta\rho_n^\sigma$ and $\Delta\rho_e^\sigma$ can both provide a moderately accurate prediction of η, although the accuracy is better if an EDL thickness based on $\Delta\rho_e^\sigma$ is used. The fact that EDL thickness based on $\Delta\rho_n^\sigma$ gives a poorer prediction of η is expected, because EDL capacitance is most directly related to the change of space charge density rather than ion number density as the electrode is electrified. Another more subtle reason is as follows. As shown in Fig. 7, $\Delta\rho_e^\sigma$ is significantly affected by the change in anion concentration as the electrode is electrified even near electrodes with negative surface charge density (similar phenomenon has also been found in our earlier studies[9]). Hence, $\Delta\rho_{n,\text{counter-ion}}^\sigma$ profile is a poor metric for the change of EDL structure and $\Delta\rho_e^\sigma$ as an electrode is electrified, which in turn leads to poorer prediction of the EDL capacitance.

Table 1 The EDL thickness based on different choices described in the text of Section 4.2 and comparison of curvature-induced capacitance enhancement predicted by eqn (6) and MD simulations

Counter-ion	BMIM$^+$		BMIM$^+$		Cl$^-$		PF$_6^-$	
Co-ion	Cl$^-$		PF$_6^-$		BMIM$^+$		BMIM$^+$	
$d_\infty(d_c)$ based on:	$\Delta\rho_n$	$\Delta\rho_e$	$\Delta\rho_n$	$\Delta\rho_e$	$\Delta\rho_n$	$\Delta\rho_e$	$\Delta\rho_n$	$\Delta\rho_e$
d_∞/nm	*0.44*	0.34	*0.41*	0.33	*0.31*	0.31	*0.39*	0.29
d_c (nm)	*0.39*	0.35	*0.39*	0.33	*0.33*	0.33	*0.39*	0.29
$\eta = C_c/C_\infty$ eqn (6)	*1.70*	1.42	*1.58*	1.44	*1.35*	1.35	*1.51*	1.39
$\eta = C_c/C_\infty$ (MD)	1.30		1.43		1.44		1.33	

In summary, the above discussions suggest that, despite the rich structure of EDLs in ILs, if the EDL thickness is suitably parameterized (in particular, if the EDL thickness is based on the change of space charge density as the electrode is electrified), the Helmholtz and xEDCC models can predict the EDL capacitance with reasonable accuracy.

5. A new theoretical model for EDLs in ILs

Although the Helmholtz and xEDCC models can predict EDL capacitance values with reasonable accuracy, they constitute quite crude simplifications of the actual EDLs in ILs. The fundamental assumption of these models is that the electrode charge is screened by a single layer of counter-ions adsorbed on the electrode surface and the electrolytes beyond this single layer are structureless. This assumption is in contradiction with the alternating layering of counter-ion/co-ions observed in ILs. It is therefore desirable to develop more elaborate models for the EDLs in ILs. Prior studies have led to interesting models for EDLs in ILs from mean-field theories. However, due to the complicated nature of EDLs in ILs, a number of assumptions had to be made in a mean-field approach, *e.g.*, ion–ion correlations are neglected to a large extent. Consequently, some important features of the EDLs cannot be described by these models. Here we take a more phenomenological approach with the objective of capturing key features of the EDLs observed in MD simulations.

As shown in Fig. 2, 3, 5, and 7, the alternating layering of ions adjacent to the electrode is one key feature of the EDLs in ILs. The layer alternation becomes weaker as the position moves further from the electrode. The overscreening of electrode charge is another key feature of the EDLs in ILs. It is known that, in concentrated ionic systems, the strong ion–ion interactions can lead to overscreening of the electrode charge. The overscreening of electrode charge in ILs was perhaps first envisioned by Kornshev and was subsequently observed in a model IL made of charged Lennard-Jones spheres.[8,14,17] In our current simulations, in which the ILs are modeled with chemical details (*e.g.*, complex shape and charge delocalization), we also observed similar phenomena. To quantify the charge overscreening, we introduce a charge screening factor

$$\beta_\infty(z) = -\int_0^z \Delta\rho_e^\sigma(s)\mathrm{d}s/\sigma, \tag{7}$$

near planar electrodes, and

$$\beta_c(r) = -\int_R^r \frac{s}{R}\Delta\rho_e^\sigma(s)\mathrm{d}s/\sigma, \tag{8}$$

near cylindrical electrodes. At position with $\beta > 1.0$, the electrode charge is overscreened. Fig. 8 shows the charge screening factor β near planar and CNT electrodes with

View Online

Downloaded by University of Tennessee at Knoxville on 26 November 2010
Published on 15 November 2010 on http://pubs.rsc.org | doi:10.1039/C0CP02077J

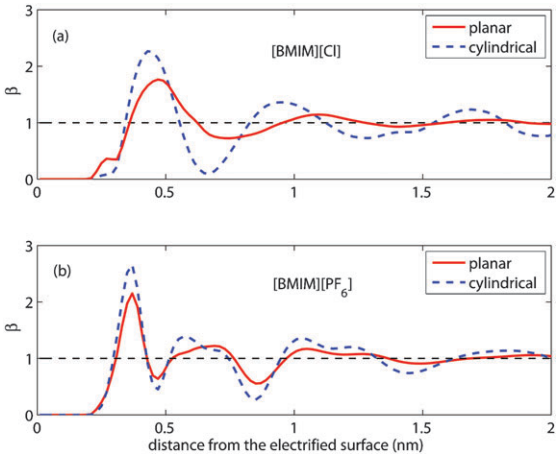

Fig. 8 The charge screening factor β in [BMIM][Cl] (panel a) and [BMIM][PF_6] (panel b) near negative planar/cylindrical electrodes. The electrode charge density is -0.112 C m^{-2} in all cases.

$\sigma = -0.112$ C m^{-2}. We observe that β always exceeds 1.0 at a position near the first counter-ion concentration peak (see Fig. 3 and 5). Beyond this position, β oscillates around 1.0 and the oscillation becomes weaker as the distance from the electrode increases. Similar trends have also been observed in the simulations of [BMIM][NO_3] and [BMIM][BF_4].[54] Therefore, we conclude that the overscreening of electrode charge is a universal feature of the EDLs in ILs.

In this work, we propose a "Multiple Ion Layers with Overscreening" (MILO) model for the EDLs in ILs to take into account the alternating layering of ions adjacent to the electrode and the overscreening of the electrode charge. Fig. 9 shows a schematic of the MILO model. In essence, we assume that the EDL consists of a counter-ion layer that overscreens the electrode charge and an adjacent co-ion layer. The counter-ion layer is located at a distance S_p from the electrode, and the net charge of this layer is $-\beta A\sigma$, where β is the charge overscreening factor at position S_p. σ and A are the charge density and area of the electrode surface, respectively. The excess charge of the counter-ion layer is balanced exactly by the adjacent co-ion layer located at position S_s from the counter-ion layer. Note that the layering of ions beyond the first two layers is much weaker and is therefore neglected. Using elementary electrostatic theory, the capacitance of EDLs near planar and CNT electrodes described by the MILO model is found to be

$$C_\infty = \frac{\varepsilon_\infty}{S_p^\infty - (\beta_\infty - 1)S_s^\infty}, \tag{9}$$

$$C_c = \frac{\varepsilon_c}{R\left[\ln\left(1+\frac{S_p^c}{R}\right) - (\beta_c - 1)\ln\left(1+\frac{S_s^c}{R+S_p^c}\right)\right]}, \tag{10}$$

where the superscripts ∞ and c denote planar and cylindrical electrodes, respectively. Note that in the limit of $\beta = 1$, eqn (9) and (10) reduce to eqn (3) and (4), respectively. The parameters of eqn (9) and (10) include S_p, S_s and β. The value of S_p and S_s can be deduced from the size of the counter-ions and co-ions. Determining β, however, is more difficult. In principle, β can be derived from more advanced models. In this work, we focus on the predicting power of eqn (9) and (10) for the EDL capacitance for a given value of β. To test eqn (9) and (10) based on the MILO model, we again adopt the approach used in Section 4 to circumvent the difficulty of obtaining precise value of dielectric constant in EDLs by studying the enhancement of EDL capacitance due to electrode curvature. Specifically, assuming $\varepsilon_c \approx \varepsilon_\infty$, eqn (9) and (10) predict that the enhancement of EDL capacitance by the electrode curvature follows:

$$\eta = \frac{C_c}{C_\infty} = \frac{S_p^\infty - (\beta_\infty - 1)S_s^\infty}{R\left[\ln\left(1+\frac{S_p^c}{R}\right) - (\beta_c - 1)\ln\left(1+\frac{S_s^c}{R+S_p^c}\right)\right]}. \tag{11}$$

The predicted enhancement of EDL capacitance near a CNT electrode over that near a planar electrode, η, is compared to that computed directly from MD simulations in Table 2. We observe that the relative error of prediction by eqn (11) is about 5% except for EDLs in [BMIM][Cl] adjacent to electrode with $\sigma = -0.112$ C m^{-2}, where the relative error is about 14%.

The agreement between the MD data and the prediction made with eqn (11) suggests that the MILO model is capable of capturing some of the essential physics of EDLs in ILs. Although the accuracy of the prediction by eqn (11) is comparable to that of the Helmholtz/xEDCC models, the new model can potentially explain other phenomena that are difficult to explain within the framework of these prior models. For example, eqn (11) predicts that charge overscreening tends to lead to an increase in EDL capacitance. Since charge

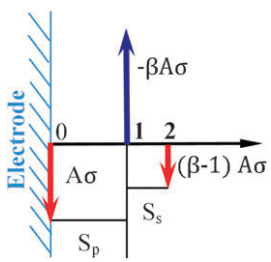

Fig. 9 A schematic of the "multiple ion layers with overscreening" (MILO) model. The charge of the electrode ($A\sigma$), the first counter-ion layer ($-\beta A\sigma$), and the adjacent co-ion layer ($(\beta - 1)A\sigma$) are assumed to be localized at positions 0, 1 and 2.

Table 2 Key parameters of the MILO model measured in MD simulations and comparison of curvature-induced capacitance enhancement predicted by eqn (6) and MD simulations

Counter-ion Co-ion	$BMIM^+$ Cl^-	$BMIM^+$ PF_6^-	Cl^- $BMIM^+$	PF_6^- $BMIM^+$
β_∞	1.76	2.08	2.26	1.86
β_c	2.25	2.60	2.73	2.56
S_p^∞/nm	0.47	0.37	0.36	0.33
S_s^∞/nm	0.16	0.06	0.15	0.04
S_p^c/nm	0.45	0.37	0.37	0.34
S_s^c/nm	0.10	0.06	0.17	0.03
$\eta = C_c/C_\infty$ (eqn (11))	1.48	1.49	1.38	1.39
$\eta = C_c/C_\infty$ (MD)	1.30	1.43	1.44	1.33
Relative error (%)	13.8	4.2	4.2	5.3

 This journal is © the Owner Societies 2010

View Online

Downloaded by University of Tennessee at Knoxville on 26 November 2010
Published on 15 November 2010 on http://pubs.rsc.org | doi:10.1039/C0CP02077J

overscreening generally decreases as the electrode potential (or the electrode surface charge density) increases,[17] eqn (11) provides a possible way for understanding the decreased capacitance of EDLs as the electrode potential increases, which is hard to achieve using the classical Helmholtz model, since the EDL thickness is known to change little as the electrode potential changes.[9] The next step in developing the MILO model is to compute the overscreening factor β self-consistently without using MD simulations, and work along this line is currently under way.

6. Conclusions

We studied the structure and capacitance of the EDLs at planar and cylindrical electrodes modeled by graphene sheets and carbon nanotubes in ILs with $BMIM^+$ cations and Cl^-/PF_6^- anions using MD simulations and density functional theory. The size of the anions is found to affect the position/height of the $BMIM^+$ ion concentration peak near both positive and negative electrodes. At the most fundamental level, these effects stem from the different attractions between cations and anions with different sizes. However, regardless of the anion size, overscreening of the electrode charge was observed in all the EDLs studied, suggesting that it is a universal feature of the EDLs in ILs. For EDLs with different counter-ions, we found that the capacitance of the EDLs follows the order: $BMIM^+$ (Cl^- as co-ion) $\approx$ $BMIM^+$ (PF_6^- as co-ion) $\approx$ PF_6^- $<$ Cl^- near both planar and cylindrical electrodes. For the same electrolyte and electrode charge density, the EDL capacitance is higher near cylindrical electrodes. These trends are consistent with the expectations from the Helmholtz and xEDCC models. Using the EDL structure and capacitance data obtained from the MD simulations, we examined the accuracy of the Helmholtz and xEDCC models, and found that, if the EDL thickness is suitably parameterized, these models can predict the EDL capacitance with good accuracy despite the dramatically simplified EDL structure assumed.

To account for the two critical features of the EDLs in ILs, namely, the alternating layering of cations and anions near the electrode and the overscreening of electrode charge, we propose a "Multiple Ion Layers with Overscreening" (MILO) model for the EDLs in ILs. The capacitance computed from the MILO model agrees well with the MD prediction, although at present, some input parameters of the MILO model must be obtained from MD simulations. However, we emphasize that the MILO model provides a new framework for understanding many interesting and important aspects of EDLs in ILs, in particular, the dependence of EDL capacitance on the electrode potential, which is very difficult to rationalize using the classical EDL models.

Acknowledgements

The authors at Clemson acknowledge support from NSF under grant No. CBET-0967175 and also thank the Clemson-CCIT office for providing computer time. R.Q. was partly supported by an appointment to the HERE program for faculty at the Oak Ridge National Laboratory (ORNL) administered by Oak Ridge Institute for Science and Education (ORISE). B.G.S., J.H., and V.M. gratefully acknowledge the support from the Laboratory Directed Research and Development Program of ORNL that helped support the initial phase of the study of the energy storage properties of ionic liquids inside carbon nanotubes and the Center for Nanophase Materials Sciences (CNMS), sponsored by the Division of Scientific User Facilities, U. S. Department of Energy, for supporting the work exploring the fundamental interfacial interactions of ionic liquids within nanoconfined graphitic systems. S.D. was supported as part of the Fluid Interface Reactions, Structures and Transport (FIRST) Center.

References

1 H. Ohno, *Electrochemical Aspects of Ionic Liquids*, John Wiley and Sons, Inc., New York, 2005.
2 M. Ue, T. Takeda, T. Takahashi and M. Takehara, *Electrochem. Solid-State Lett.*, 2002, **5**, A119.
3 C. Nanjundiah, S. F. McDevitt and V. R. Koch, *J. Electrochem. Soc.*, 1997, **144**, 3392.
4 M. Kosmulski and B. Tendaj, *Przem. Chem.*, 2001, **80**, 280.
5 T. Welton, *Chem. Rev.*, 1999, **99**, 2071.
6 M. T. Alam, M. M. Islam, T. Okajima and T. Ohsaka, *J. Phys. Chem. C*, 2008, **112**, 2601.
7 C. Pinilla, M. G. Del Pópolo, J. Kohanoff and R. M. Lynden-Bell, *J. Phys. Chem. B*, 2007, **111**, 4877.
8 M. V. Fedorov and A. A. Kornyshev, *J. Phys. Chem. B*, 2008, **112**, 11868.
9 G. Feng, J. S. Zhang and R. Qiao, *J. Phys. Chem. C*, 2009, **113**, 4549.
10 V. Lockett, R. Sedev, J. Ralston, M. Horne and T. Rodopoulos, *J. Phys. Chem. C*, 2008, **112**, 7486.
11 S. Baldelli, *Acc. Chem. Res.*, 2008, **41**, 421.
12 B. L. Bhargava and S. Balasubramanian, *J. Am. Chem. Soc.*, 2006, **128**, 10073.
13 M. Sha, F. Zhang, G. Wu, H. Fang, C. Wang, S. Chen, Y. Zhang and J. Hu, *J. Chem. Phys.*, 2008, **128**, 134504.
14 A. A. Kornyshev, *J. Phys. Chem. B*, 2007, **111**, 5545.
15 K. B. Oldham, *J. Electroanal. Chem.*, 2008, **613**, 131.
16 A. A. Kornyshev, S. Leikin and G. Sutmann, *Electrochim. Acta*, 1997, **42**, 849.
17 M. V. Fedorov and A. A. Kornyshev, *Electrochim. Acta*, 2008, **53**, 6835.
18 J. Huang, B. G. Sumpter and V. Meunier, *Chem.–Eur. J.*, 2008, **14**, 6614.
19 A. Berthod, J. J. Kozak, J. L. Ding, J. L. Anderson and D. W. Armstrong, *Theor. Chem. Acc.*, 2007, **117**, 127.
20 W. D. Cornell, P. Cieplak, C. I. Bayly, I. R. Gould, K. M. Merz, D. M. Ferguson, D. C. Spellmeyer, T. Fox, J. W. Caldwell and P. A. Kollman, *J. Am. Chem. Soc.*, 1995, **117**, 5179.
21 N. M. Micaelo, A. M. Baptista and C. M. Soares, *J. Phys. Chem. B*, 2006, **110**, 14444.
22 J. N. C. Lopes, J. Deschamps and A. A. Pádua, *J. Phys. Chem. B*, 2004, **108**, 2038.
23 E. Lindahl, B. Hess and D. van der Spoel, *J. Mol. Model.*, 2001, **7**, 306.
24 B. Hess, H. Bekker, H. Berendsen and J. Fraaije, *J. Comput. Chem.*, 1997, **18**, 1463.
25 G. Feng, J. Huang, B. G. Sumpter, V. Meunier and R. Qiao, *Phys. Chem. Chem. Phys.*, 2010, **12**, 5468.
26 J. N. Sachs, P. S. Crozier and T. B. Woolf, *J. Chem. Phys.*, 2004, **121**, 10847.
27 S. Wang, S. Li, Z. Cao and T. Yan, *J. Phys. Chem.C*, 2010, **114**, 990.
28 G. Kresse and J. Hafner, *Phys. Rev. B: Condens. Matter*, 1993, **47**, 558.
29 G. Kresse and J. Hafner, *Phys. Rev. B: Condens. Matter*, 1994, **49**, 14251.
30 G. Kresse and J. Furthmuller, *Comput. Mater. Sci.*, 1996, **6**, 15.

View Online

Downloaded by University of Tennessee at Knoxville on 26 November 2010
Published on 15 November 2010 on http://pubs.rsc.org | doi:10.1039/C0CP02077J

31 G. Kresse and J. Furthmuller, *Phys. Rev. B: Condens. Matter*, 1996, **54**, 11169.
32 G. Kresse and D. Joubert, *Phys. Rev. B: Condens. Matter Mater. Phys.*, 1999, **59**, 1758.
33 P. E. Blochl, *Phys. Rev. B: Condens. Matter*, 1994, **50**, 17953.
34 J. P. Perdew, K. Burke and M. Ernzerhof, *Phys. Rev. Lett.*, 1996, **77**, 3865.
35 S. A. Kislenko, I. S. Samoylov and R. H. Amirov, *Phys. Chem. Chem. Phys.*, 2009, **11**, 5584.
36 P. Du, S. Liu, P. Wu and C. X. Cai, *Electrochim. Acta*, 2007, **52**, 6534.
37 G. D. Smith, O. Borodin, S. P. Russo, R. J. Rees and A. F. Hollenkamp, *Phys. Chem. Chem. Phys.*, 2009, **11**, 9884.
38 S. Wang, Z. Cao, S. Li and T. Lan, *Sci. China Chem.*, 2009, **52**, 1434.
39 J. Israelachvili, *Intermolecular and Surface Forces*, Academic Press, New York, 1992.
40 J. H. Antony, D. Mertens, T. Breitenstein, A. Dölle, P. Wasserscheid and W. R. Carper, *Pure Appl. Chem.*, 2004, **76**, 255.
41 G. Raabe and J. Köhler, *J. Chem. Phys.*, 2008, **128**, 154509.
42 K. Dong, S. J. Zhang, D. X. Wang and X. Q. Yao, *J. Phys. Chem. A*, 2006, **110**, 9775.
43 T. Koddermann, C. Wertz, A. Heintz and R. Ludwig, *ChemPhysChem*, 2006, **7**, 1944.
44 W. Zhao, F. Leroy, B. Heggen, S. Zahn, B. Kirchner, S. Balasubramanian and F. Müller-Plathe, *J. Am. Chem. Soc.*, 2009, **131**, 15825.
45 S. K. Reed, O. J. Lanning and P. A. Madden, *J. Chem. Phys.*, 2007, **126**, 084704.
46 J. Huang, B. G. Sumpter, V. Meunier, G. Yushin, C. Portet and Y. Gogotsi, *J. Mater. Res.*, 2010, **25**, 1469.
47 V. Ballenegger and J.-P. Hansen, *J. Chem. Phys.*, 2005, **122**, 114711.
48 H. Weingärtner, P. Sasisanker, C. Daguenet, P. J. Dyson, I. Krossing, J. Slattery and T. Schubert, *J. Phys. Chem. B*, 2007, **111**, 4775.
49 T. Singh and A. Kumar, *J. Phys. Chem. B*, 2008, **112**, 12968.
50 B. E. Conway, J. O'M. Bockris and I. A. Ammar, *Trans. Faraday Soc.*, 1951, **47**, 756.
51 J. R. MacDonald and C. A. Barlow, Jr., *J. Chem. Phys.*, 1962, **36**, 3062.
52 J. Dzubiella and J.-P. Hansen, *J. Chem. Phys.*, 2005, **122**, 234706.
53 O. Teschke and E. F. de Souza, *Appl. Phys. Lett.*, 1999, **74**, 1755.
54 G. Feng and R. Qiao, unpublished data.

 This journal is © the Owner Societies 2010